Published: 7th October 2026

ANACHEM JOURNAL
ISSN: 2006-5221 (Online)

CATALYTIC EFFICIENCY OF ACID-IMPREGNATED AND UNIMPREGNATED SOLID CATALYSTS ON BIODIESEL PRODUCTION USING UNCONVENTIONAL INDIGENOUS SEED OILS

[*1]Ndubuisi, J.O., [2]Ekpunobi, U.E., [3]Princewill, O.A., [4]Umeokoli, B.O., [1]Ezeagwu, P.C., [2]Okonkwo, P.C., [2]Modozie, B.U., and [2]Aghanwa, C.I.

[1]Department of Biochemistry, Federal University of Allied Health Sciences, Enugu State, Nigeria
[2]Department of Pure and Industrial Chemistry, Nnamdi Azikiwe University, Awka. Anambra State, Nigeria
[3]Shanahan University, Onitsha, Anambra State, Nigeria
[4]Department of Pharmaceutical and Medicinal Chemistry, Nnamdi Azikiwe University, Awka, Anambra State, Nigeria
[*]Corresponding author's e-mail: ndubuisijulie@gmail.com
https://doi.org/10.5281/zenodo.23147739

ABSTRACT

With the increasing demand for renewable energy worldwide, efficient catalysts for biodiesel production have become a research focus. As the renewable energy market grows, research on efficient catalysts to produce biodiesel from local feedstocks is also gaining momentum. Acid-impregnated and unimpregnated solid catalysts derived from marine animal shells were tested for biodiesel production using three underutilized indigenous seed oils: fluted pumpkin (Telfairia occidentalis), chia (*Salvia hispanica*), and pumpkin (Cucurbita pepo). Oils were extracted using Soxhlet extraction with n-hexane. Acid values ranged from 0.17 to 20.20 mg KOH/g (FFA: 0.09%–10.10%), and iodine values ranged from 16.4 to 296.2 g I_2/100 g. Sea shells were calcined at 900 °C for 2 hours, impregnated with a concentrated H_2SO_4 solution, dried in air at 120 °C for 12 h, and recalcined at 500 °C for 3 hours to produce the acid-impregnated catalysts. The characterization of the catalysts was carried out using Scanning Electron Microscopy (SEM), FTIR, and XRF. FTIR confirmed –SO_3H groups at 1040 cm^{-1} and 1180 cm^{-1}, and XRF detected sulfur only in the sulfonated catalysts (3.27–3.59 wt% SO_3). Biodiesel was produced by transesterification, and the process was optimized using a five-level, four-factor Central Composite Design (CCD) comprising 50 runs for each oil. Optimal conditions were: catalyst dose 2.25 wt%, methanol/oil 10:1, 50 °C, 3 h, 300 rpm. FAME content was determined by GC-FID following ISO/TS 17307 with identification by retention-time comparison against authenticated standards. The maximum FAME content was 81.6% for fluted pumpkin oil and 84.4% for both chia and pumpkin oils. Models were significant ($p < 0.0001$; $R^2 = 0.8715–0.8800$). The FAME content in the bio-oils produced was higher with acid-impregnated catalysts than with unimpregnated catalysts, particularly for high-FFA oils. The measured biodiesel properties were compared with the limits specified in ASTM D6751 and EN 14214, and all fell within the required ranges: density 0.87–0.89 g/cm^3, viscosity 4.2–4.8 mm^2/s, flash point > 120 °C, acid value 0.25–0.30 mg KOH/g, and pour point –4 to –6 °C. The results support using local seed oils and low-cost, acid-impregnated seashell catalysts to produce sustainable biodiesel.

Keywords: Renewable; acid-impregnated catalyst; Underutilized seed oils; Transesterification

1.0. Introduction

Rising global energy demand has made energy provision an increasingly pressing issue for energy security, sustainability, and the economy. Global energy demand remains predominantly based on fossil fuels; however, because they are finite, highly consumed, and rapidly depleting, there is a growing global search for alternative renewable and sustainable energy (Arjoon & Speight, 2021; Bisht & Pandey, 2025). Fossil-fuel combustion is a major source of greenhouse gas emissions and a driver of climate change and environmental degradation, posing risks to people's health, well-being, and future economic development (Awasthi & Shanmugam, 2022; Singla et al., 2023). Biofuels, especially biodiesel, have the following properties, which make them attractive today: renewable, biodegradable, and non-polluting (Chauhan et al., 2023). Among them, biodiesel increases cetane number, reduces sulphur content, and lowers particulate matter emissions (Babatunde et al., 2024).

The EDF is non-toxic and biodegradable, unlike fossil diesel, where all CO_2 produced as a combustion product is released into the atmosphere. EDF is based on non-toxic, biodegradable products and operates in a closed carbon cycle, meaning that plants reabsorb all CO_2 produced during combustion through photosynthesis (Awasthi & Shanmugam, 2022). Biodiesel use causes less environmental damage and reduces dependence on imported oil compared with fossil fuels (Rajamehala et al., 2022). However, biodiesel commercialization faces challenges: transesterification catalysts do not produce high yields, and bio-oil has high feedstock and production costs (Dhawane & Halder, 2019). Virtually all biodiesel feedstocks are edible vegetable oils already used for conventional biodiesel production: soybean oil, palm oil, and rapeseed oil (Babatunde et al., 2024). This dependency has contributed to the increasingly frivolous 'food versus fuel' dilemma, where countries turn to food sources that traditionally had non-food uses in developing countries for fuel production, becoming proportionally more vulnerable to food insecurity (Bisht & Pandey, 2025).

Edible oil is fairly expensive, further increasing manufacturing costs, which is why it is less competitive than fossil diesel biodiesel (Raina et al., 2024). Therefore, researchers are studying new and unconventional oil sources as future fuel options (Rajamehala et al., 2022; Rayeen et al., 2026).

Nigeria has many local oil crops, such as pumpkin (Cucurbita pepo), fluted pumpkin (Telfairia occidentalis), and chia (Salvia hispanica), that have not been tapped as energy crops. They can be used directly as food products, but Nigeria does not currently use them as biofeedstocks for bio-oil production because they are locally abundant and do not compete directly with staple food crops. They would also be more economical and contribute to the valorization of agricultural products in the region (Raut et al., 2025; Babu et al., 2026). A key challenge in biodiesel production is catalyst efficiency, and the chemical process of producing fatty acid methyl esters (FAMEs) from oils is called transesterification and requires a catalyst (Dhawane & Halder, 2019).

Homogeneous alkaline catalysts, such as sodium hydroxide and potassium hydroxide, are widely used because of their high catalytic activity and reaction rate (Singh et al., 2022). These catalysts, however, do tend to cause soap formation in cases of relatively high concentrations of free fatty acids (FFA) in the feedstock, have limited recoverability of the catalyst, and produce significant

quantities of wastewater during purification of the product process (Dhawane & Halder, 2019; Rajamehala et al., 2022). These disadvantages limit biodiesel production, increase production costs, and cause environmental problems.

In lieu of homogeneous catalysts, researchers have investigated solid heterogeneous catalysts because they are reusable and produce minimal wastewater, which is easy to separate from the catalyst (Dhawane & Halder, 2019). However, many heterogeneous catalysts have low activity, particularly with a high level of FFAs (found in non-conventional oils) in the feedstock (Rajamehala et al., 2022). To address this limitation, researchers have studied several modifications of solid catalysts based on acid impregnation (Neme et al., 2022). This method provides an acidic surface, increasing active-site density, improving catalytic efficiency, and facilitating simultaneous esterification and transesterification. Acid-impregnated solid catalysts from natural materials such as animal bones, seashells, etc. have been seen to perform well, especially for feedstocks with high concentrations of FFAs (Dhawane & Halder, 2019).

In coastal areas of Nigeria, researchers observed and extracted several species of these waste materials, such as *Pinctada margaritifera, Charonia tritonis*, and *Acanthocardia aculeata*, for use as cheap, sustainable catalyst precursors (Alsabi et al., 2024). These applications may include waste management and the use of local resources in accordance with circular economy principles (Babu et al., 2026). A literature search on using acid-impregnated shell catalysts to produce biodiesel from locally sourced Nigerian seed oils found no studies on this application. Although numerous studies have examined biodiesel production using conventional catalysts and oil sources, few have compared the performance of an acid-impregnated catalyst with an unimpregnated or solid catalyst, particularly when using indigenous Nigerian oils. Moreover, researchers have investigated the effect of such optimized catalysts on biodiesel production, reaction kinetics, and fuel properties only for a few oils with varying FAA, such as fluted pumpkin, chia, and pumpkin oil (Onoji, 2017; Yazilitaş et al., 2024).

Although numerous studies have investigated biodiesel production using conventional catalysts and feedstocks, there is no study that directly compared the acid-impregnated and unimpregnated solid catalysts derived from three species of Nigerian seashells (*Pinctada margaritifera*, *Charonia tritonis*, and *Acanthocardia aculeata*) with the production of three underutilized indigenous feedstocks for biodiesel production (Dhawane & Halder, 2019; Rajamehala et al., 2022). The novelty of the work comes in three ways: (1) Three different species of seashells were used separately as catalyst precursors; (2) The acid-impregnated seashell was compared with the unimpregnated one; (3) Three different types of indigenous oils with varying FFA contents were tested while optimizing the reaction parameters for each oil using a 5-level, 4-factor CCD.

Overcoming this gap is vital to improve biodiesel research and move closer to utilizing local feedstocks while reducing reliance on imported catalysts and technologies. The three neglected indigenous seed oils (ISOs) used for investigating the catalytic efficiency of these seashell catalytic materials (acid-impregnated and unimpregnated) are for biodiesel production. The effect of catalyst modification on biodiesel yield was investigated; biodiesel was characterized for essential fuel properties and lipid products, and the results were compared with ASTM D6751 and EN 14214 standards.

2.0. Materials and Methods

2.1. Materials and Reagents

The chemicals used comprised n-hexane (for oil extraction), methanol (99.5% purity), concentrated sulfuric acid (H_2SO_4, 98% purity), anhydrous sodium sulfate, ethanol, petroleum ether, potassium hydroxide (KOH), sodium hydroxide (NaOH), hydrochloric acid (HCl), potassium iodide (KI), sodium thiosulfate ($Na_2S_2O_3$), phenolphthalein indicator, starch indicator, and Wijs solution. Distilled and deionized water was used for all applications involving water. No chemical purification was performed.

The following equipment was used: Soxhlet extraction apparatus, rotary evaporator, muffle furnace, magnetic stirrer with hot plate, three-necked round-bottom flask (500 mL), reflux condenser, separating funnel, analytical balance, oven, desiccator, Ostwald viscometer, and Pensky-Martens closed-cup flash point tester.

The instrumental analysis methods employed were Scanning Electron Microscopy (SEM) with Energy-Dispersive X-ray Analysis (EDX), Fourier Transform Infrared Spectroscopy (FTIR), Gas Chromatography–Flame Ionization Detection (GC-FID), and X-ray Fluorescence (XRF).

2.2. Collection of Feedstock and Oil Extraction

Seeds of Telfairia occidentalis, popularly called fluted pumpkin; Salvia hispanica, commonly known as chia; and Cucurbita pepo, commonly referred to as pumpkin, were procured from a local market, Awka, Anambra State, Nigeria. The harvested seeds were cleaned of dislodged soil and, after washing in plenty of water, were air-dried at room temperature. Dried seeds were milled in a laboratory mill into a powder. Oil was extracted using the Soxhlet technique, with n-hexane as the solvent. Each 1200g seed sample was ground for each batch. The solvent was evaporated under reduced pressure at 40 °C using a rotary evaporator. The recovered oils were stored in amber glass bottles at 4 °C to protect them from oxidation before analysis. The percentage oil yield was calculated by:

$$\%\, Oil\ extracted = (Weight\ of\ oil\ extracted - Weight\ of dry\ seed) \times 100 \quad (Eq.1)$$

2.3. Catalyst Preparation

Seashell wastes from 3 species, namely *Pinctada margaritifera* (catalyst A), *Charonia tritonis* (catalyst B), and *Acanthocardia aculeata* (catalyst C), were collected from the Nigerian coasts. The shells were washed multiple times with distilled water to remove organics and sand, then dried in an oven at 105 °C for 24 hrs. The dried shells were pulverized into a powder. The powdered shells were calcined in a muffle furnace at 900 °C for 2 hours to convert calcium carbonate ($CaCO_3$) to calcium oxide (CaO), the active base material (Dhawane & Halder, 2019; Alsabi et al., 2024). The powder was then cooled in a desiccator, re-ground, and sieved to obtain a fine, uniform powder. Impregnation of shell powder with concentrated H_2SO_4 (sulfonation). The incipient wetness impregnation method (Dhawane & Halder, 2019; Neme et al., 2022) was used to impregnate the calcined shell powder with 0.1 M H_2SO_4. A weighed quantity of the powder was made into a uniform paste by adding a measured quantity of H_2SO_4 with constant stirring. The paste was dried in an oven at 120 °C for 12 h and recalcined at 500 °C for 3 h to attach sulfonic acid ($–SO_3H$) groups to the catalyst surface (Dhawane & Halder, 2019; Alsabi et al., 2024). For each catalyst, both acid-impregnated (sulfonated) and non-impregnated (calcined) forms were prepared.

2.4. Catalyst Characterization

Surface morphology of the raw, calcined, and acid-impregnated catalysts was examined by scanning electron microscopy (SEM) on a Phenom ProX SEM with a focused electron-beam acceleration voltage of 20 kV and magnification up to ×7000. Samples were sputter-coated with gold (~5nm thick) in a Quorum Q150R sputter coater and imaged.

Energy Dispersive X-ray Spectroscopy (EDX): To determine the elemental composition of the catalysts, EDX was performed on the SEM. The samples were coated with gold and analyzed under vacuum.

Fourier Transform Infrared Spectroscopy (FTIR): Functional groups in the catalysts and oils were identified using a Bulk Scientific Model 530 IR spectrometer. The liquid samples were sandwiched between two KBr disks and scanned from 600 to 4000 cm^{-1}.

X-ray Fluorescence (XRF): The elemental composition of the sulfonated and calcined (dried) catalysts was determined by X-ray Fluorescence (XRF) using a Thermo Noran spectrometer (Model: G250) with WinTrace software developed by Thermo Noran Corporation. The daily calibration was done using a copper standard. Samples were placed in sample cups and analyzed under a vacuum.

Surface area and pore parameters: The surface area, pore volume, pore density, and bulk density of the raw, calcined, and acid-impregnated catalysts were measured by N_2 adsorption.

2.5. Transesterification Procedure

All extracted oils were processed by transesterification in 500 mL 3-neck round-bottom flasks under reflux with magnetic stirring. For each experiment, the desired amount of oil (typically 50mL) was added to the reactor and agitated while the reaction temperature was maintained. The appropriate quantity of the catalyst was spread over a fixed volume of MeOH and placed in the reactor. Because methanol boils at approximately 64.7 °C, reactions conducted at or above this temperature require a validated reflux condenser and careful temperature control; otherwise, methanol loss would alter the effective methanol-to-oil molar ratio. Reaction time was determined from the time when the catalyst and the methanol were added. After the reaction, the mixture was cooled to room temperature, transferred to a separating funnel, and left for 1 hour. Two layers formed: the dark brown glycerol layer and the light-coloured, yellowish biodiesel (FAME) layer. The FAME layer was removed, rinsed gently with warm (deionized) water, dried over anhydrous sodium sulfate, and finally transferred to a dry container under an argon stream. The biodiesel yield was calculated as:

$$\%\,Yield = (Weight\ of\ FAME\ /\ Weight\ of\ oil\ used) \times 100 \quad (Eq.2)$$

2.6. Physicochemical Characterization of Oils and Biodiesel

The extracted oils and resulting biodiesel samples were characterized for the following properties using standard methods:

Acid value and FFA: 2 g of oil sample was dissolved in 50 mL of neutral solvent (petroleum ether/ethanol mixture) and stirred for 30 minutes. The mixture was titrated with 0.1 M NaOH and phenolphthalein indicator until a persistent pink endpoint appeared.

$$Acid\ value = \frac{(Titre\ value \times 5.61)}{Weight\ of\ oil\ sample)} \quad (Eq.3)$$

$$FFA\ (\%) = Acid\ value\ /\ 2 \quad (Eq.4)$$

Saponification value: 2 g of oil sample was refluxed with 25 mL of alcoholic KOH on a steam bath for 30 minutes with periodic shaking. The mixture was titrated against 0.5 M HCl using phenolphthalein indicator. A

blank determination was carried out simultaneously.

$$Saponification\ value = \frac{(b-a) \times 28.5}{Weight\ of\ sample} \quad (Eq.5)$$

where *b* = volume of HCl used in blank titration, *a* = volume of HCl used in sample titration.

Iodine value: 0.3 g of oil sample was dissolved in 10 mL of carbon tetrachloride, followed by addition of 20 mL of Wijs solution. The mixture was kept in the dark for 30 minutes, after which 15 mL of 10% KI solution and 100 mL of distilled water were added. The mixture was titrated against 0.1 M $Na_2S_2O_3$ using starch indicator. A blank was run simultaneously.

$$Iodine\ value\ = \frac{(b-a) \times 1.269}{(Weight\ of\ sample} \quad (Eq.6)$$

Moisture content: 2 g of oil sample was weighed into a pre-weighed crucible and dried in an oven at 105 °C for 3 hours, with periodic cooling and reweighing until constant weight.

$$Moisture\ content\ (\%) = \frac{(W2-W3)}{(W2-W1)} \times 100 \quad (Eq.7)$$

where W_1 = weight of empty crucible, W_2 = weight of crucible + sample before drying, W_3 = weight of crucible + sample after drying.

Specific gravity: A clean, dry 50 mL density bottle was weighed and labelled empty (M), then filled with distilled water (M_1) and with the oil or biodiesel sample (M_2). Specific gravity was calculated as:

$$Specific\ gravity\ = \frac{(W2-W1)}{(W3-W1)} \quad (Eq.8)$$

where W_1 = weight of empty bottle, W_2 = weight of bottle + sample, W_3 = weight of bottle + water.

Kinematic viscosity. An Ostwald viscometer was immersed in a temperature-controlled bath at 40 °C for 30 minutes. Flow time was recorded, and kinematic viscosity was calculated from the viscometer constant.

Flash point. Determined using a Pensky-Martens closed-cup apparatus according to ASTM D93 (Jääskeläinen, 2024). The sample was heated at approximately 5 °C/min with continuous stirring, and the lowest temperature at which a distinct flash occurred was recorded.

Cloud point and pour point. Determined according to ASTM D2500 and ASTM D97, respectively (Jääskeläinen, 2024). The sample was cooled in a controlled bath, and temperatures at which cloud formation and pour (flow) occurred were recorded.

2.7 Fatty Acid Composition by GC-FID

The fatty acid composition of oils and biodiesel samples was analysed by a GC-FID (Bulk Scientific, Model 910). The injector temperature was 250 °C, and helium was used as the carrier gas. The oven temperature program was as follows: initial temperature 50 °C (held for 1 min), heated to 325 °C at 10 °C/min, and held for 2 min. Fatty acid methyl ester identification was done by comparing retention time with authenticated standards following the procedure described in ISO/TS 17307 (International Organization for Standardization, 2016).

2.8. Experimental Design and Statistical Analysis

Optimization of transesterification was carried out using a five-level, four-factor Central Composite Design (CCD) generated with Design-Expert software (Version 12.0, Stat-Ease Inc., USA):

A = Catalyst dose (wt%)
B = Reaction time (h)
C = Reaction temperature (°C)
D = Methanol-to-oil molar ratio
The design included factorial points (2^k), axial points (2k), and replicated center points,

for a total of 50 experimental runs per oil. The response variable was FAME content (%). The second-order polynomial model used to fit the data was:

$$Y = b_0 + \Sigma b_i x_i + \Sigma b_{ii} x_i^2 + \Sigma b_{ij} x_i x_j + \varepsilon \quad (Eq. 9)$$

Analysis of variance (ANOVA) was used to evaluate the significance of model terms at the 95% confidence level ($p < 0.05$). Model adequacy was assessed using the coefficient of determination (R^2), adjusted R^2, predicted R^2, adequate precision, and coefficient of variation (CV).

3.0 Results and Discussion

3.1 Characterization of the Oil Samples

The physicochemical properties of the three extracted oils, fluted pumpkin (Oil A), chia (Oil B), and pumpkin (Oil C), are presented in Table 3.1, alongside the corresponding ASTM D6751 limits for biodiesel feedstock assessment.

Table 3.1: Physicochemical Properties of the Raw Oils

Parameter	Oil A (Fluted Pumpkin)	Oil B (Chia)	Oil C (Pumpkin)	ASTM D6751 Limit
Moisture content (%)	7.84	7.84	1.92	0.05 max
Specific gravity	1.040	0.831	0.875	0.86 – 0.90
Saponification value (mg KOH/g)	196.3	189.0	162.7	
Peroxide value (mEq/g)	48.0	12.0	36.0	
Iodine value (g I_2/100 g)	296.2	22.6	16.4	< 125
Acid value (mg KOH/g)	3.93	0.17	20.20	0.50 max
FFA (%, as oleic acid)	2.44	0.64	2.61	—
Kinematic viscosity at 40 °C (mPa·s)	10,802	95.86	180.97	1.9 – 6.0
Refractive index	1.445	1.452	1.448	
Flash point (°C)	230	240	250	130 min
Cloud point (°C)	1.2	5.0	8.0	–3 to 12

Parameter	Oil A (Fluted Pumpkin)	Oil B (Chia)	Oil C (Pumpkin)	ASTM D6751 Limit
Pour point (°C)	7.0	10.0	8.0	–15 to 10

The physicochemical property results of the three oils, as shown in Table 3.1, differ significantly and thus directly affect their viability for transesterification. The moisture contents of Oils A and B were 7.84%, respectively, and were comparatively lower in Oil C (1.92%). All three exceed the ASTM D6751 maximum of 0.05% for biodiesel, so drying is necessary before transesterification, as it promotes triglyceride hydrolysis and soap formation (Dhawane & Halder, 2019; Rajamehala et al., 2022).

The specific gravities were within the range set by ASTM for Oil C (0.875) but were outside the range for Oil A (1.040) and Oil B (0.831). This indicates that Oil C is most similar to the density properties of the biodiesel feedstock. The acid values were very high: Oil B was lowest (0.17 mg KOH/g), Oil A was intermediate (3.93 mg KOH/g), and Oil C was highest (20.20 mg KOH/g). The FFA contents were similar: 0.09%, 1.97%, and 10.10%, respectively. If FFA is calculated as oleic acid, FFA (%, as oleic acid) = acid value / 1.99. The reported acid values imply approximate FFA values of 2.44% for fluted pumpkin oil, 0.64% for chia oil, and 2.61% for pumpkin oil, moderate values, not necessarily 'high.' The FFA content of Oils A and C is fairly high, which would normally require an acid-catalyzed esterification (pretreatment) before alkaline transesterification to prevent soap formation. However, the acid-impregnated heterogeneous catalyst developed in this study was designed to perform both esterification and transesterification, so no pretreatment was needed. Soap formation is undesirable because it can lower biodiesel yields and make it harder to separate glycerol. Excess FFA also reduces catalyst efficiency and increases production costs (Rajamehala et al., 2022).

When comparing the degree of unsaturation indicated by iodine value, Oil A (296.2 g I_2/100 g) had an exceptionally high value, and Oils B (22.6) and C (16.4) had very low values. The former is interesting because chia oil is normally high in linolenic acid and should have a high iodine value, while the latter is normally moderate. The saponification values range from 162.7 to 196.3 mg KOH/g, indicating a typical triglyceride molecular weight and suggesting the oil is suitable for transesterification (Yazilitaş et al., 2024).

3.2 Fatty Acid Composition of the Oils

Table 3.2: Fatty Acid Composition of the Oils (% weight)

Fatty Acid	Carbon Number	Oil A (Fluted Pumpkin)	Oil B (Chia)	Oil C (Pumpkin)
Capric acid	$C_{10:0}$	7.29		
Lauric acid	$C_{12:0}$	12.62		
Myristic acid	$C_{14:0}$	10.24	8.02	8.02
Myristoleic acid	$C_{14:1}$		13.89	13.89
Palmitic acid	$C_{16:0}$	10.36		
Palmitoleic acid	$C_{16:1}$		11.27	11.27
Margaric acid	$C_{17:0}$		11.39	11.39
Stearic acid	$C_{18:0}$	10.28	10.38	10.38
Oleic acid	$C_{18:1}$	9.93	11.32	11.32
Linoleic acid	$C_{18:2}$	8.53	10.93	10.93
Arachidic acid	$C_{20:0}$	10.90		
Eicosatetraenoic acid	$C_{20:4}$		11.99	11.99
Docosadienoic acid	$C_{22:2}$	10.74		
Docosahexaenoic acid	$C_{22:6}$	9.11	11.82	11.82
Total saturated		61.69	29.79	29.79
Total unsaturated		38.31	46.06	46.06

Table 3.2 presents the fatty acid profiles of the three oils, determined by GC-FID. Saturated fatty acids (61.69%) predominated in oil A (mostly lauric, arachidic, palmitic, stearic, and myristic), while the unsaturated fraction (38.31%) comprised oleic, linoleic, docosadienoic, and docosahexaenoic acids. This highly saturated profile would likely produce biodiesel with very good oxidative stability but very poor cold-flow properties. Oils B and C were similar, with around 30% saturated and 46% unsaturated fatty acids.

Eicosatetraenoic, myristoleic, palmitoleic, oleic, linoleic, and docosahexaenoic acids were the most abundant unsaturated ones. The fatty acid profiles are comparable to those reported for oils normally used in biodiesel production (Yazilitaş et al., 2024). Seed oil composition varies by cultivar, geography, storage, and extraction method; broad ranges require chromatographic evidence. For Oils B and C, unsaturated fats can improve fluidity and cold-flow behaviour but may compromise oxidative stability (Awasthi & Shanmugam, 2022). The high linolenic-acid content of chia oil is relevant to oxidative stability: EN 14214 limits linolenic acid methyl ester content and specifies oxidation stability requirements, rather than merely treating high unsaturation as favorable. Oil A's profile is highly saturated, favours stability, but may adversely affect cold flow.

3.3 Catalyst Characterization

3.3.1 Scanning Electron Microscopy (SEM)

SEM micrographs of the raw and acid-impregnated catalysts (Catalysts A, B, and C) were recorded at ×7000 magnification (Figures 3.1–3.6). The images revealed clear morphological differences among the three catalyst forms.

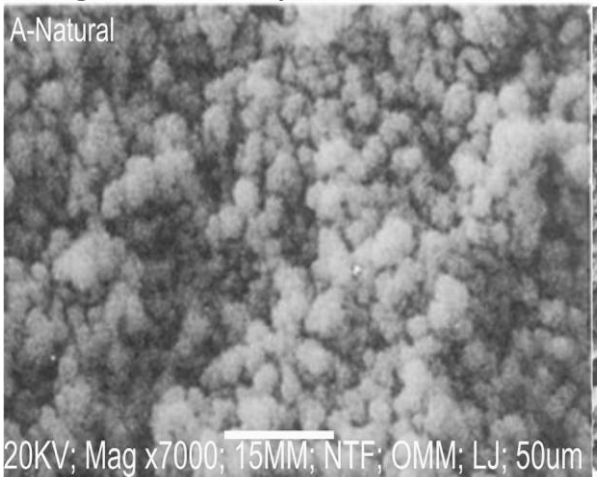

Figure 3.1: SEM micrograph of raw Catalyst A

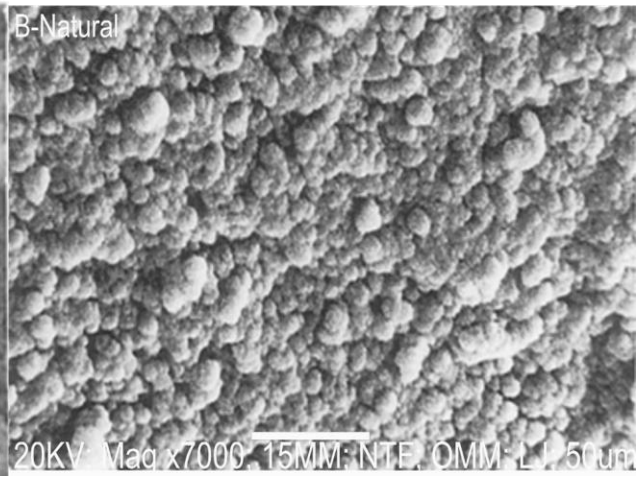

Figure 3.2: SEM micrograph of raw Catalyst B

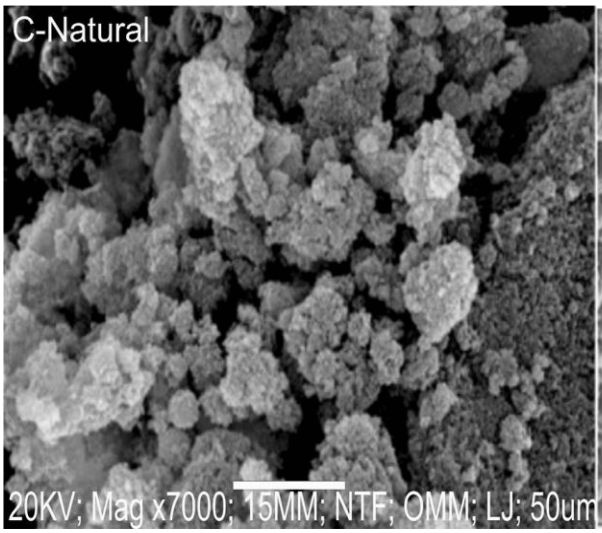

Figure 3.3: SEM micrograph of raw Catalyst C

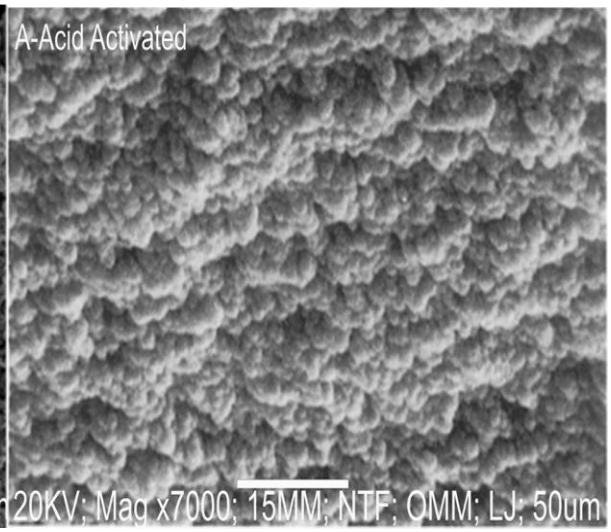

Figure 3.4: SEM micrograph of acid-impregnated Catalyst A

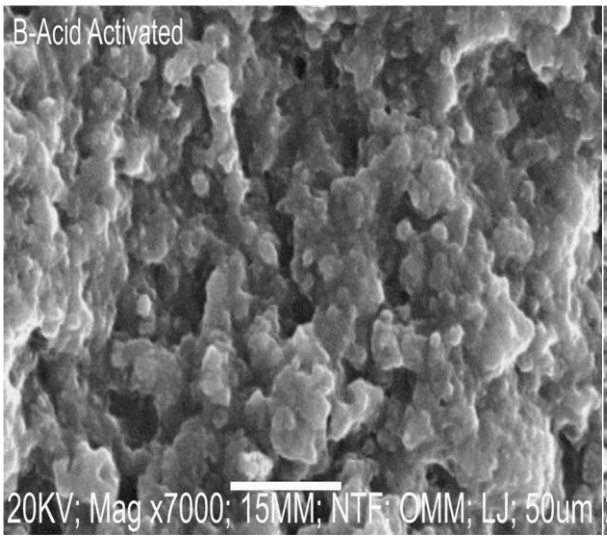

Figure 3.5: SEM micrograph of acid-impregnated Catalyst B

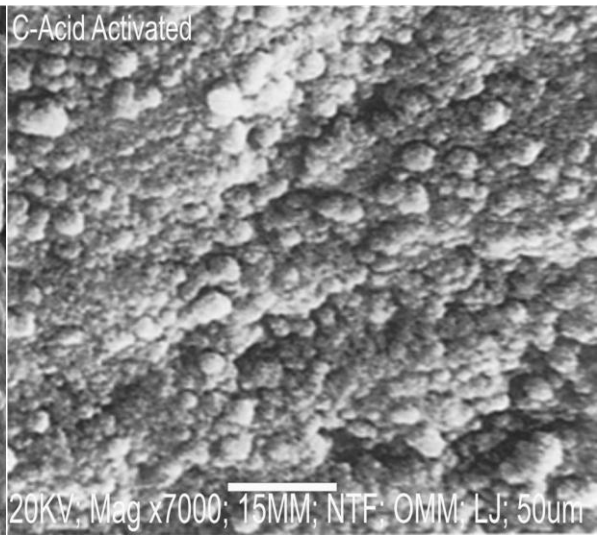

Figure 3.6: SEM micrograph of acid-impregnated Catalyst C

Shell powders were irregularly shaped, compact, and low in porosity. The resulting particles were then calcined at 900 °C, yielding an open, connected, porous granular structure that was also advantageous for catalytic activity. The surface texture of acid-impregnated catalysts was even rougher than that of raw catalysts, and had even greater porosity. The surface roughening is attributed to impregnation with sulphonic acid (–SO_3H), consistent with the incorporation of acid functional groups observed by FTIR. Although SEM alone cannot quantify surface area or active site density, the observed increase in surface roughness is consistent with previously reported morphological changes in acid-functionalized catalysts (Dhawane & Halder, 2019).

3.3.2. Fourier Transform Infrared Spectroscopy (FTIR)

FTIR spectra of the calcined and sulfonated catalysts (Table 3.3) confirmed the presence of the expected functional groups.

Table 3.3: FTIR Absorption Bands of Calcined and Sulfonated Catalysts

Wavenumber (cm^{-1})	Assignment	Catalyst Form
3640	Surface hydroxyl / adsorbed water	Calcined
1415	Carbonate species (possible $CaCO_3$)	Calcined
1180	Sulfate species (consistent with, not proof of $–SO_3H$)	Sulfonated
1040	Sulfate species (consistent with, not proof of $–SO_3H$)	Sulfonated

Calcined catalysts had well-defined bands at 3640 cm^{-1} and 1415 cm^{-1}. A band near 3640 cm^{-1} is more plausibly associated with surface hydroxyl groups or adsorbed water, not a Ca–O vibration, since Ca–O lattice vibrations occur mainly in the low-wavenumber region. A band near 1415 cm^{-1} may indicate carbonate species, especially because CaO readily reacts with atmospheric CO_2 to form $CaCO_3$, and should not automatically be assigned as Ca–O bending.

The sulfonated catalysts also showed additional peaks at 1180 cm^{-1} and 1040 cm^{-1}. Bands near 1040–1180 cm^{-1} can be consistent with sulfate species, but this alone does not prove surface $–SO_3H$ groups. This functionalization is expected to improve catalyst functionality by facilitating not only esterification of FFAs but also transesterification of triglycerides (Dhawane & Halder, 2019; Neme et al., 2022).

3.3.3. X-ray Fluorescence (XRF)

XRF analysis of the calcined and sulfonated catalysts (Table 3.4) identified CaO as the major component in all calcined shell catalysts, with only minor amounts of Mg, Si, and Fe.

Table 3.4: XRF Analysis of Calcined and Sulfonated Shell Catalysts (wt%)

Component	Calcined Catalyst A	Calcined Catalyst B	Calcined Catalyst C	Sulfonated Catalyst A	Sulfonated Catalyst B	Sulfonated Catalyst C
CaO	65–72	65–72	65–72	60–68	60–68	60–68
Mg (as MgO)	< 1.0	< 1.0	< 1.0	< 1.0	< 1.0	< 1.0

Component	Calcined Catalyst A	Calcined Catalyst B	Calcined Catalyst C	Sulfonated Catalyst A	Sulfonated Catalyst B	Sulfonated Catalyst C
Si (as SiO_2)	< 0.5	< 0.5	< 0.5	< 0.5	< 0.5	< 0.5
Fe (as Fe_2O_3)	< 0.5	< 0.5	< 0.5	< 0.5	< 0.5	< 0.5
S (as SO_3)	Not detected	Not detected	Not detected	3.27	3.59	

Calcination of each catalyst did not result in sulfur, but sulfur was detected in the sulfonated catalysts (3.27–3.59 wt% as SO_3). XRF commonly reports elemental oxides but cannot directly identify $-SO_3H$ surface groups; 'S as SO_3 / $-SO_3H$' is not an appropriate direct XRF assignment. Bands near 1040–1180 cm^{-1} in FTIR can be consistent with sulfate species, but this alone does not prove surface $-SO_3H$ groups. After sulfonation, the product's CaO content slightly decreased (from 65–72 wt% to 60–68 wt%), corresponding to the introduction of $-SO_3H$ groups that dilute the CaO fraction. These $-SO_3H$ groups also enhance the acidity of the catalyst surface and make high-FFA oils suitable for esterification, thus overcoming a major limitation of base catalysts (Dhawane & Halder, 2019; Alsabi et al., 2024). The small amounts of Mg, Si, and Fe show that the calcined shells are mostly CaO, consistent with the thermal decomposition of $CaCO_3$.

3.4. Elemental Composition (EDX) and Surface Properties

All the raw, calcined, and acid-activated catalysts (Table 3.5) contained catalytically relevant elements Ca, Mg, K, P, and Na for the catalysis reactions studied, in addition to C and O elements, typical of the organic-mineral origin of the shell precursors.

Table 3.5: Elemental Composition of Raw, Sulfonated, and Calcined Catalysts (wt%)

Element	Raw A	Raw B	Raw C	Sulfonated A	Sulfonated B	Sulfonated C	Calcined A	Calcined B	Calcined C
O	7.30	4.46	5.46	7.56	7.54	7.24	13.20	7.52	35.0
C	3.22	3.20	3.24	3.22	3.26	3.25	2.29	3.20	20.0

Element	Raw A	Raw B	Raw C	Sulfonated A	Sulfonated B	Sulfonated C	Calcined A	Calcined B	Calcined C
K	4.30	4.22	4.22	4.12	4.10	4.10	4.15	4.10	1.25
Mg	2.27	3.20	3.25				5.74	3.29	
P	23.45		2.35					23.47	
Ca	56.50	24.52		3.45	27.20	16.52	20.32	55.46	1.31
Si		57.44	78.52	75.42	9.35	62.96	51.96		85.60
S				3.27		3.59			5.20
Na					2.40				1.12
Fe									3.30
N									17.50

The presence of Ca, Mg, K, and Na indicates that the catalysts are alkali/alkaline-earth group minerals, which are essential for transesterification activity (Dhawane & Halder, 2019; Alsabi et al., 2024). Carbon and oxygen indicate organic and carbonate rocks. Certain samples show a high concentration of silicon (from the sand/shell matrix), which may contribute to structural stability. The detection of sulfur in sulfonated catalysts confirms the XRF analysis and further indicates successful sulfonation.

3.5 Optimization of Transesterification for Oil A (Fluted Pumpkin)

The transesterification of Oil A was optimized using a 50-run D-optimal, 5-level, four-factor Central Composite Design (CCD), as presented in Table 3.7. The

variables that were affecting the reaction were varied independently and included catalyst dose (A), agitation speed (B), reaction time (C), methanol-to-oil molar ratio (D), and reaction temperature (E). The dependent variable was FAME content (%). The amount of FAME varied from 30.5% at the edge point to 81.6% at the center point (2.25 wt.%, 3 hours, 50 °C, 10:1, 300 rpm).

Table 3.7: ANOVA for Response Surface Model Oil A Biodiesel

Source	Sum of Squares	df	Mean Square	F-value	p-value	Significance
Model	8053.05	20	402.65	9.83	< 0.0001	significant
A: Catalyst dose	209.53	1	209.53	5.12	0.0314	
B: Reaction time	16.14	1	16.14	0.394	0.5351	
C:Temperature	239.44	1	239.44	5.85	0.0221	
D:Methanol/Oil	759.91	1	759.91	18.56	0.0002	
E: Reaction speed	261.24	1	261.24	6.38	0.0173	
A^2	2250.10	1	2250.10	54.94	< 0.0001	
B^2	2036.64	1	2036.64	49.73	< 0.0001	
C^2	2613.76	1	2613.76	63.82	< 0.0001	
D^2	1420.06	1	1420.06	34.68	< 0.0001	
E^2	590.89	1	590.89	14.43	0.0007	
Residual	1187.64	29	40.95			
Lack of Fit	1101.88	22	50.09	4.09	0.0313	significant
Pure Error	85.76	7	12.25			
Cor Total	9240.68	49				

Model summary: $R^2 = 0.8715$; Adjusted $R^2 = 0.7828$; Predicted $R^2 = 0.4911$; Adequate Precision = 10.7030; CV = 11.34%. The second-order polynomial model obtained in terms of coded variables was:

$$\text{FAME content} = 80.35 + 2.20A - 0.61B + 2.35C + 4.19D + 2.46E - 6.36A^2 - 6.05B^2 - 6.86C^2 - 5.06D^2 - \ldots \quad \text{(Eq. 3.1)}$$

where A = catalyst dose, B = reaction time, C = temperature, D = methanol/oil ratio, and E = agitation speed. The positive sign in front of a term indicates a synergistic effect, while a negative sign indicates an antagonistic effect.

This is supported by an F-value of 9.83 with a probability level of less than 0.0001. The coefficient of determination (R^2 = 0.8715) shows that 87.15% of the variation in FAME is explained by this model, and the adjusted R^2 (0.7828) indicates the model is not overfitted. The CV is low (11.34%), which means that the experimental data are reliable.

For the linear terms, the methanol-to-oil ratio (D) was the most important positive term, followed by catalyst dose (A), temperature (C), and agitation speed (E). Reaction time (B) did not significantly affect the response linearly. (p = 0.5351). All quadratic terms were significant, with a negative sign implying that FAME content increased quadratically to a maximum and then decreased, as in a classic response surface. The lack-of-fit test was significant (p = 0.0313), so the model may not fit the system's behaviour. This is a shortcoming of the present model and should be kept in mind when predicting beyond the observed range. This could be due to the complexity of the reaction system, unmeasured noise factors, or other unconsidered factors.

For the model, the R-squared value is lower at 0.4911, compared with the adjusted R-squared of 0.7828. If the difference between these values is >0.2, this can mean a large block effect or issues with the model and/or data. The amount of FAME rose as the amount of catalyst was increased until around 2.25 wt%, after which no further improvement was seen. Too much catalyst can cause emulsion and viscosity problems and make mass transfer difficult.

The molar ratio of FAME content was increased to 10:1. Above 3.5, glycerol separation became difficult, resulting in lower apparent FAME content. Here, 6:1 is mentioned, which is probably to scale up the reaction to reduce FFA formation and offset methanol loss during the reaction. The optimum temperature was 50 °C; higher temperatures accelerated the reaction so much that saponification and methanol loss became important. Methanol boils at approximately 64.7 °C; therefore, reactions conducted at or above 70 °C require a validated reflux setup and careful temperature control, since methanol loss would otherwise alter the effective methanol-to-oil molar ratio.

3.6. Optimization of Transesterification for Oil B (Chia)

A five-level, four-factor Central Composite Design (CCD) comprising 50 experimental runs was used to optimize transesterification of Oil B as presented in Table 3.8. The observed FAME content ranged from 34.4% to 84.4%, with a maximum of 84.4% obtained at the center-point conditions (catalyst dose 2.25 wt%, time 3 h, temperature 50 °C, methanol/oil 10:1).

Table 3.8: ANOVA for Response Surface Model: Oil B Biodiesel

Source	Sum of Squares	df	Mean Square	F-value	p-value	Significance
Model	7793.15	20	389.66	10.63	< 0.0001	significant
A: Catalyst dose	224.92	1	224.92	6.14	0.0193	
B: Reaction time	13.65	1	13.65	0.3725	0.5464	
C: Temperature	201.59	1	201.59	5.50	0.0261	
D: Methanol/Oil	737.43	1	737.43	20.12	0.0001	
E: Reaction speed	290.40	1	290.40	7.92	0.0087	
AD	170.20	1	170.20	4.64	0.0396	
A^2	2029.96	1	2029.96	55.38	< 0.0001	
B^2	2041.86	1	2041.86	55.70	< 0.0001	
C^2	2639.95	1	2639.95	72.02	< 0.0001	
D^2	1288.57	1	1288.57	35.15	< 0.0001	
E^2	606.62	1	606.62	16.55	0.0003	
Residual	1063.08	29	36.66			
Lack of Fit	999.86	22	45.45	5.03	0.0176	significant
Pure Error	63.22	7	9.03			
Cor Total	8856.23	49				

The model is significant, with an F-value of 10.63 and $p < 0.0001$. The R-squared is 0.8800, meaning the model accounted for 88.00% of the variance in FAME content, and the adjusted R-squared is 0.7972, indicating the model was not overfitted. The CV (10.12%) is low and therefore indicates good experimental reliability.

The methanol-to-oil ratio (D) again had the greatest effect on the linear term, followed by the catalyst dose (A), agitation speed (E), and temperature (C). This second factor, reaction time (B), was not significant ($p = 0.5464$). All quadratic terms were significant and negative, again demonstrating the classical optimum behaviour. The interaction term AD (catalyst dose × methanol/oil ratio) was significant ($p = 0.0396$), meaning the effect of catalyst dose on FAME content depends on the methanol-to-oil ratio.

This interaction is expected - greater methanol concentration will help drive the reaction, and greater catalyst will increase the reaction. The lack of fit was significant ($p = 0.0176$), and the Predicted R^2 (0.5191) was also very low compared to the Adjusted R^2 (0.7972). Both of these impressions imply the model may not entirely reflect all (the full) variation.

3.7 Optimization of Transesterification for Oil C (Pumpkin)

A five-level, four-factor CCD with 50 runs was used to optimize transesterification of Oil C, as shown in Table 3.9. The observed FAME content ranged from 34.4% to 84.4%, with a maximum of 84.4% obtained at the center-point conditions.

Table 3.9: ANOVA for Response Surface Model (Oil C Biodiesel)

Source	Sum of Squares	df	Mean Square	F-value	p-value	Significance
Model	7408.45	20	370.42	9.10	< 0.0001	significant
A: Catalyst dose	238.55	1	238.55	5.86	0.0220	
B: Reaction time	10.19	1	10.19	0.2503	0.6207	
C:Temperature	210.27	1	210.27	5.17	0.0306	
D: Methanol/Oil	737.92	1	737.92	18.13	0.0002	
E: Reaction speed	297.75	1	297.75	7.31	0.0113	
AD	195.03	1	195.03	4.79	0.0368	
A^2	1809.70	1	1809.70	44.46	< 0.0001	

Source	Sum of Squares	df	Mean Square	F-value	p-value	Significance
B^2	1917.78	1	1917.78	47.11	< 0.0001	
C^2	2511.79	1	2511.79	61.71	< 0.0001	
D^2	1204.08	1	1204.08	29.58	< 0.0001	
E^2	577.24	1	577.24	14.18	0.0008	
Residual	1180.44	29	40.70			
Lack of Fit	1109.56	22	50.43	4.98	0.0181	significant
Pure Error	70.88	7	10.12			
Cor Total	8588.89	49				

The results are significant with an F-value of 9.10 ($p < 0.0001$). The models for both oils A and B are similar, with $R^2 = 0.8626$ and Adjusted $R^2 = 0.7678$. The CV (10.05%) is good, with excellent experimental reliability.

The linear trends and significant linear parameters were comparable to those for Oils A and B: the methanol-to-oil ratio (D) was again the most significant linear parameter, followed by catalyst dose (A), agitation rate (E), and temperature (C). Reaction time (B) showed no significant difference ($p = 0.6207$). All the quadratic terms have negative signs and are significant. The interaction AD was also significantly different ($p = 0.0368$). Again, lack of fit was significant ($p = 0.0181$), and the Predicted R^2 (0.4491) was lower than the Adjusted R^2 (0.7678), indicating the same relationship observed for Oils A and B.

3.8. Comparison of the Three Oils

Across the three oils, the optimal transesterification conditions were identical: catalyst dose 2.25 wt%, methanol/oil molar ratio 10:1, reaction temperature 50 °C, reaction time 3 h, and agitation speed 300 rpm. Table 3.10 presents the maximum FAME contents.

Table 3.10: Maximum FAME Content by Oil

Oil	Maximum FAME content (%)
Oil A (Fluted pumpkin)	81.6
Oil B (Chia)	84.4
Oil C (Pumpkin)	84.4

Oil B and Oil C had slightly higher FAME contents than Oil A (84.4% vs. 81.6%). The difference is small (~3%, and it is likely that this variation is attributable to their difference in fatty acid composition, FFA content, or small matrix differences during reaction.

Oil A gave the highest acid value (3.93 mg KOH/g), and oils B and C had comparatively low and high FFA levels (0.17 and 20.20 mg KOH/g), respectively, but both produced the maximum FAME value. The acid-impregnated catalyst demonstrated compatibility and effectiveness for transesterification and simultaneous esterification over a broad range of ester feed fatty acid (FF.A.) contents. The differences in maximum FAME content among the three oils are also small, suggesting that the acid-impregnated seashell catalyst is effective with a variety of oil feedstocks. This is practically important for biodiesel production in Nigeria, as it allows a single catalyst to be used with multiple oils.

3.9. Fuel Properties of the Biodiesel

Table 3.11 summarizes the physicochemical fuel properties of biodiesel produced from the three oils using the acid-impregnated catalysts, alongside the ASTM D6751 and EN 14214 specifications.

Table 3.11: Fuel Properties of Biodiesel Compared with ASTM D6751 and EN 14214

Property	Unit	Biodiesel Value	ASTM D6751	EN 14214
Density at 15 °C	g/cm³	0.87 – 0.89	0.86 – 0.90	0.86 – 0.90
Viscosity at 40 °C	mm²/s	4.2 – 4.8	1.9 – 6.0	3.5 – 5.0
Flash point	°C	> 120	≥ 93	≥ 120
Acid value	mg KOH/g	0.25 – 0.30	≤ 0.50	≤ 0.50
Pour point	°C	–4 to –6	Not specified	Not specified

All measured fuel properties fell within the limits specified by ASTM D6751 and EN 14214.

4.0. Conclusion

This work aimed to compare the performance of acid-impregnated and unimpregnated solid catalysts synthesized from the shells of various seafood in catalysing biodiesel production from three underutilised indigenous seed oils: fluted pumpkin (Telfairia occidentalis), chia (Salvia hispanica), and pumpkin seed (*Cucurbita pepo*). Waste seashells were processed in two steps to prepare catalysts: Calcination to 900 °C and acid impregnation with concentrated H_2SO_4. FTIR confirmed the presence of sulfonic acid ($–SO_3H$) groups, and XRF detected sulfur only in the sulfonated catalysts.

SEM revealed that the surface roughness and porosity of the calcined and acid-impregnated shell powder were greater than those of the raw shell powder. The physicochemical properties of the three oils differed significantly. The acid value ranged from 0.17–20.20 mg KOH/g (FFA: 0.09–10.10%), which severely tested catalyst performance under both low- and high-FFA feedstocks. Acid-impregnated catalysts exhibited good activity on all three oils, showing activity towards both FFA esterification and the transesterification of triglycerides, a notable property compared to base catalysts, which saponify high-FFA feedstocks. Optimization of transesterification was done by adopting a five-level, four-factor Central Composite Design (CCD). All three oils gave similar optimum conditions: catalyst dose: 2.25 wt%, Methanol-to-oil ratio: 10:1, Temperature: 50 °C, reaction time: 3 h, and Agitation speed: 300 rpm. Maximum FAME contents were 81.6% (fluted pumpkin), 84.4% (chia), and 84.4% (pumpkin). ANOVA models were significant ($p < 0.0001$) for all three oils, with R^2 values of 0.8715, 0.8800, and 0.8626, respectively. In all three cases, the methanol-to-oil ratio was the most important variable, and reaction time had no significant linear effect.

Acid-impregnated catalysts achieved higher FAME levels than the unimpregnated catalyst, and the best results were achieved for the high-FFA oils, where soap formation was limited. This showed the effectiveness of acid impregnation as a modification method for shell-derived solid catalysts. The biodiesel fulfilled the main quality requirements from ASTM D6751 and EN 14214. Density (0.87–0.89 g/cm³), kinematic viscosity at 40 °C (4.2–4.8 mm²/s), flash point (> 120 °C), acid value (0.25–0.30 mg KOH/g), and pour point (–4 to –6 °C) all fell within the specified limits. The results indicate that this biodiesel fuel is fit for use in blending with conventional diesel fuel when produced using the acid-impregnated seashell catalysts extracted from indigenous oils.

References

Alsabi, H. A., Shafi, M. E., Almasoudi, S. H., Mufti, F. A. M., Alowaidi, S. A., Sharawi, S. E., and Alaswad, A. A. (2024). From waste to catalyst: Transforming mussel shells into a green solution for biodiesel production from Jatropha curcas oil. Catalysts, 14(1), 59. https://doi.org/10.3390/catal14010059

Arjoon, K. K., & Speight, J. G. (2021). Biofuels. In Sustainable solutions for environmental pollution: Waste management and value-added products (Vol. 1, pp. 163–198). Wiley.

Awasthi, D., & Shanmugam, K. T. (2022). Advanced biofuels: Perspectives and possibilities. In Advanced biofuel technologies (pp. 21–38). Elsevier.

Babatunde, E. O., Ebhodaghe, S. O., & Owoyale, F. B. (2024). Biomass-derived materials: Biofuel production. In Handbook of advanced biomass materials for environmental remediation (pp. 197–221). Springer Nature Singapore.

Babu, A. S., Chakka, A. K., & Sankarganesh, P. (2026). Biomass materials as potential sources of future sustainability. Conversion and Utilization of Wastes into Sustainable Products, 1, 25–52.

Bisht, G. S., & Pandey, S. (2025). Biofuels for a sustainable future: Generations, technologies, and key challenges in renewable energy. *Bioenergy Research*, 18(1), 43.

Chauhan, M., Vanshika, Kumar, A., Chauhan, D., & Jain, A. K. (2023). Renewable feedstocks for biofuels. In Biofuel extraction techniques (pp. 151–176). Wiley.

Dhawane, S. H., & Halder, G. (2019). Synthesis of catalyst support from waste biomass for impregnation of catalysts in biofuel production. In Advances in feedstock conversion technologies for alternative fuels and bioproducts (pp. 199–220). Woodhead Publishing.

Jääskeläinen, H. (2024). Biodiesel standards and properties. DieselNet. https://dieselnet.com/tech/fuel_biodiesel_std.php

Neme, I., Gonfa, G., & Masi, C. (2022). Activated carbon from biomass precursors using phosphoric acid: A review. *Heliyon,* 8(12), e11940.

Onoji, S. E. (2017). Synthesis of biodiesel from rubber seed oil for internal compression ignition engine [Doctoral dissertation, University of the Witwatersrand].

Raina, N., Chuetor, S., Charoenkool, P., Jiradechakorn, T., Sereenonchai, C., Phojaroen, J., & Singh, H. M. (2024). Opportunities and challenges in the production of biofuels from waste biomass. In Waste valorization for bioenergy and bioproducts (pp. 23–43). Woodhead Publishing.

Rajamehala, M., Kaviprabha, A., Pandian, A. M. K., Singh, M. V. P., Karthikadevi, S., Gopalakrishnan, B., & Chozhavendhan, S. (2022). Lignocellulosic biomass as an alternate source for next-generation biofuel. In Biofuels and bioenergy (pp. 207–221). Elsevier.

Raut, S. S., Sharma, A., & Mishra, A. (2025). Valorization of wheat residue to biofuels and chemicals. In Valorization of solid wastes to biofuels and chemical products for sustainable world (pp. 203–223). Springer Nature Singapore.

Rayeen, F., Garg, P., Dhankani, P., Gupta, A., Singh, P., Singh, P. K., & Pathak, N. (2026). Biofuels from lignocellulosic biomass: Challenges, technological bottlenecks, applications, and future perspectives. In Biofuels from lignocellulosic biomass (pp. 51–86). Woodhead Publishing.

Singh, R., Pooja, L. R., Tomer, R., & Shukla, A. (2022). Current state of the art of lignocellulosic biomass: Future biofuels. In Status and future challenges for non-conventional energy sources, 2, 1–17. Springer.

Singla, A., Singh, Y., Abd Rahim, E., & Kumar, N. (2023). Challenges and future prospects of biofuel. In Biowaste and biomass in biofuel applications (p. 49). CRC Press.

Yazilitaş, C., Yilbaşi, Z., & Yeşilyurt, M. K. (2024). Optimization of biodiesel synthesis using non-edible hempseed oil. *Science and Technology for Energy Transition,* 79, 11.